JGP Journal of General Physiology

RESEARCH ARTICLE

cAMP binds to closed, inactivated, and open sea urchin HCN channels in a state-dependent manner

Vinay Idikuda, Weihua Gao, Zhuocheng Su, Qinglian Liu, and Lei Zhou

Hyperpolarization-activated cyclic-nucleotide–modulated (HCN) channels are nonselective cation channels that regulate electrical activity in the heart and brain. Previous studies of mouse HCN2 (mHCN2) channels have shown that cAMP binds preferentially to and stabilizes these channels in the open state—a simple but elegant implementation of ligand-dependent gating. Distinct from mammalian isoforms, the sea urchin (spHCN) channel exhibits strong voltage-dependent inactivation in the absence of cAMP. Here, using fluorescently labeled cAMP molecules as a marker for cAMP binding, we report that the inactivated spHCN channel displays reduced cAMP binding compared with the closed channel. The reduction in cAMP binding is a voltage-dependent process but proceeds at a much slower rate than the movement of the voltage sensor. A single point mutation in the last transmembrane domain near the channel's gate, F459L, abolishes inactivation and concurrently reverses the response to hyperpolarizing voltage steps from a decrease to an increase in cAMP binding. ZD7288, an open channel blocker that interacts with a region close to the activation/inactivation gate, dampens the reduction of cAMP binding to inactivated spHCN channels. In addition, compared with closed and "locked" closed channels, increased cAMP binding is observed in channels purposely locked in the open state upon hyperpolarization. Thus, the order of cAMP-binding affinity, measured by the fluorescence signal from labeled cAMP, ranges from high in the open state to intermediate in the closed state to low in the inactivated state. Our work on spHCN channels demonstrates intricate state-dependent communications between the gate and ligand-binding domain and provides new mechanistic insight into channel inactivation/desensitization.

Introduction

Hyperpolarization-activated cyclic-nucleotide–modulated (HCN) channels that encode I_f or I_h current were first isolated from cardiac myocytes and neurons (DiFrancesco, 1985; Lüthi and McCormick, 1998). Four mammalian HCN isoforms, HCN1–HCN4, and a sea urchin isoform, spHCN, have been cloned and extensively studied (Gauss et al., 1998; Ludwig et al., 1998; Santoro et al., 1998). Both native and heterologously expressed HCN channels exhibit unique biophysical properties including activation upon membrane hyperpolarization, permeability for K^+ and Na^+ ions, and a direct sensitivity to intracellular cAMP. In the absence of cAMP, spHCN channels are distinct in showing voltage-dependent inactivation. cAMP binding abolishes spHCN inactivation and makes the channel behave just like the mammalian isoforms. At the cellular level, HCN channels contribute to the maintenance of resting membrane potential, synaptic transmission, integration of dendritic signaling, and generation and propagation of action potentials. At the physiological level, HCN channels are involved in the maintenance of normal heart rate, working memory and motor learning, and inflammatory and neuropathic pain sensation (Robinson and Siegelbaum, 2003; Craven and Zagotta, 2006; Biel et al., 2009).

At the molecular level, each functional HCN channel contains four subunits. Within each subunit, there is a transmembrane domain with six α-helices homologous to that of the K_v channel, the C-linker, and the intracellular cyclic-nucleotide–binding domain (CNBD) downstream from the transmembrane domain. Crystal structures of the C-linker–CNBD fragments from mouse HCN2 and human HCN4 afford an atomic view of local interactions between cAMP and CNBD and the assembly of four protomers (Zagotta et al., 2003; Xu et al., 2010; Lolicato et al., 2011). The cryo-EM structure of HCN1 provides the first atomic view of the whole molecule (Lee and MacKinnon, 2017). These structural advances can be used as a solid platform for further experimental and computational investigations.

Many details regarding how HCN channels open, close, and inactivate (spHCN) remain unclear. As for other ion channels,

Department of Physiology and Biophysics, School of Medicine, Virginia Commonwealth University, Richmond, VA.

Correspondence to Lei Zhou: lzhou@vcu.edu.

it remains challenging to delineate the communication among adjacent and distant subdomains within the channel molecule and how they respond to membrane hyperpolarization and cAMP binding. Dynamic, state-dependent interactions between cAMP and the full-length channel protein have been demonstrated in mouse HCN2 (mHCN2) channels (Kusch et al., 2010; Wu et al., 2011). Patch-clamp fluorometry (PCF), which enables simultaneous electrical recording of channel function and optical recording of fluorescently labeled ligand in contact with the channel, offers a powerful approach to investigate the dynamic interaction between the functioning channel and ligands (Zheng and Zagotta, 2003; Biskup et al., 2007). Using fluorescent cAMP as marker for binding, it was shown that cAMP preferably binds to and stabilizes HCN2 channels in the open state and shifts the equilibrium from resting to open state (Kusch et al., 2010, 2011; Wu et al., 2011). Furthermore, based on observations with the open channel blocker ZD7288 and mutagenesis, it was proposed that a rotation of the last transmembrane segment (S6) and residues located close to the activation gate allosterically regulate cAMP binding (Wu et al., 2012). Later studies provided consistent evidence that the state-dependent binding of cAMP is likely implemented through a structural coupling mechanism involving the elongated α-helix from S6 to the C-linker region and a coordination of the four subunits (Kusch et al., 2011; Nache et al., 2013; Lee and MacKinnon, 2017). Notably, using fluorescently labeled cAMP to study cAMP-dependent gating is not a perfect approach, especially when the existence of the fluorophore alters the ligand-binding affinity and gating efficacy. To a certain extent, this line of research on ligand binding is comparable to the studies of voltage sensor movement using optical methods, which provided useful mechanistic information but ran into limitations such as the replacement of arginine or lysine by cysteine and sensitivity of the attached fluorophore to the local chemical environment.

In the presence of cAMP, spHCN shares key biophysical features with, and behaves just like, mammalian HCN channels (Gauss et al., 1998). Studies on spHCN have provided important insights into the structure–function relationship of HCN channels, such as the movement of S4 during channel activation and coupling of the gate to cAMP binding, and ultimately to channel opening (Männikkö et al., 2002, 2005; Shin et al., 2004; Bruening-Wright et al., 2007). However, in the absence of cAMP, spHCN undergoes fast voltage-dependent inactivation that has been attributed to "slippery" coupling between the gate and the movement of the voltage sensor. Here, we used fluorescent-labeled cAMP and PCF to investigate the binding of cAMP to the inactivated spHCN channel and the intriguing allosteric communication between the binding of cAMP and the gate in three different states: closed, inactivated, and open.

Materials and methods

Functional expression in *Xenopus laevis* oocytes and electrophysiological characterization

The complementary DNA encoding spHCN was generously provided by Dr. Reinhard Seifert and Dr. U. Benjamin Kaupp from the Center of Advanced European Studies and Research and inserted into the pGHEM vector for expression in *X. laevis* oocytes. The mMessage machine kit (Ambion) was used for complementary RNA synthesis. Complementary RNA (25–30 ng) encoding the spHCN channel was injected into each oocyte at stage VI. For excised patch recordings, the electrode solution (extracellular) and bath solution (intracellular) were symmetrical and contained 110 mM KCl, 2 mM NaCl, 10 mM HEPES, and 1 mM EDTA (pH 7.4 adjusted by KOH). EDTA was omitted from the bath solution when Cd^{2+} was added to keep the channel in the locked-open or locked-closed state. All experiments were performed at room temperature (22°C).

PCF

The PCF setup was constructed based on an Olympus IX71 microscope equipped with a 100× oil immersion objective lens (Plan N 100×, numerical aperture 1.25; Olympus). A 473-nm diode-pumped solid-state laser (Ultralasers Inc.) was used as the excitation light source. The following filter sets were used to collect the FITC fluorescence signal: exciter, D480/30; dichroic mirror, DC505LP; emitter, D510LP (Chroma Technology). Optical signals were detected by a 16-bit electron-multiplying charge-coupled device camera (Cascade 1K; Photometrics Inc.). Patch clamp recording was conducted with an A-M Systems (model 2400) amplifier, and current signals were filtered at 5 kHz and digitized by Digidata 1320A (Axon Instruments) at 10 kHz. The laser light source, charge-coupled device (CCD) camera exposure, and patch-clamp amplifier were synchronized by transistor–transistor logic pulses. Current recordings were not leak subtracted. Pipets drawn from KIMAX-51 glass were ∼5–10 µm in diameter with a resistance of ∼0.8 MΩ. WinWCP (created by John Dempster, University of Strathclyde) was used for data acquisition.

Maximal microscopic current traces were collected in the presence of a saturating concentration of 10 µM cAMP and a hyperpolarizing voltage step sufficient to produce maximal channel opening based on the Boltzmann equation. The optical signals were collected within the linear range of the CCD camera. ImageJ (National Institutes of Health) was used to analyze the fluorescence images (Schneider et al., 2012). ΔF was the mean fluorescence intensity in the region of interest with the background fluorescence subtracted. The ΔF values were normalized by the intensity before the hyperpolarizing voltage step (ΔΔF).

8-nitrobenzoxadiazole-cAMP (NBD-cAMP; Fig. 1 A) and 8-FITC-cAMP (FITC-cAMP) were ordered from Axxora. NBD-cAMP was not as effective as unlabeled cAMP in opening spHCN channels (Fig. 1 B). The specific binding of NBD-cAMP to the CNBD of the spHCN channel was confirmed by competition binding assay (Fig. 1 C). Fig. S1 shows the membrane fluorescence intensity as a function of NBD-cAMP concentration.

Statistics

All statistical tests were performed using OriginPro. Data are presented as mean ± SEM, and statistical significance was assessed with an unpaired *t* test. $P < .05$ was considered statistically significant, and significance is indicated as follows: ***, $P < 0.001$; **, $P < 0.01$; *, $P < 0.05$.

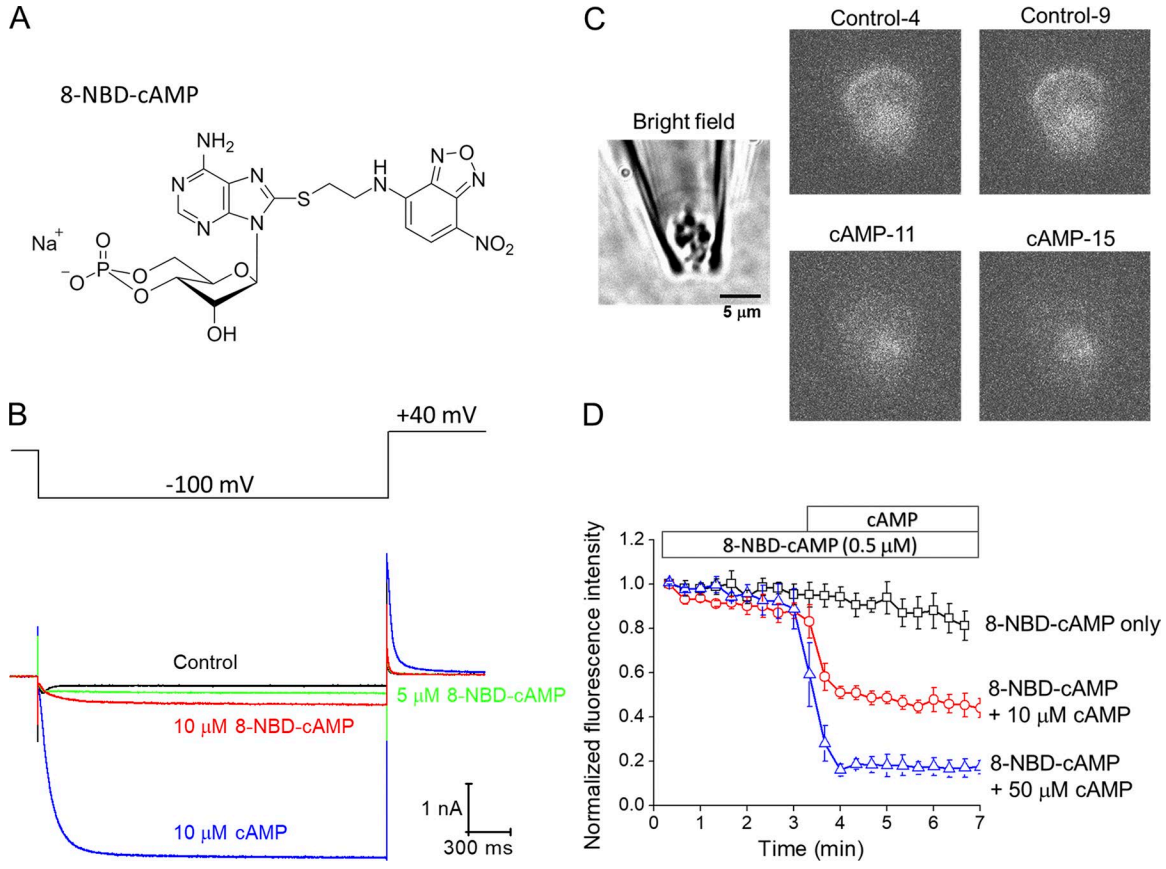

Figure 1. **Chemical structure of NBD-cAMP and the modulation of WT spHCN channels. (A)** Chemical structure of the NBD-cAMP (Axxora). **(B)** Top: Voltage protocol. Bottom: Current traces of the WT spHCN channel recorded in the absence of cAMP (black), 5 μM NBD-cAMP (green), 10 μM NBD-cAMP (red), or 10 μM regular cAMP (blue). **(C)** Competitive binding assay for the specificity of NBD cAMP binding to spHCN channels. Raw fluorescent images of membrane patch showing a decrease in the 0.5-μM NBD-cAMP fluorescence signal upon addition of saturating concentration of 50 μM nonfluorescent cAMP. **(D)** Normalized fluorescent intensities from competitive binding experiments. The fluorescence intensity of NBD-cAMP (black, control, $n = 5$) decreased upon adding regular cAMP (red, 10 μM, $n = 6$; blue, 50 μM, $n = 6$). Error bars here and after represent SEM (see Statistics in Materials and methods).

Online supplemental material

Fig. S1 shows binding of spHCN channels to NBD-cAMP at different concentrations. Fig. S2 shows NBD-cAMP binding to a mutant channel, spHCN/H462A, that is insensitive to photodynamic modification. Figs. S3 and S4 show results of using FITC-cAMP as the marker for cAMP binding to WT spHCN channels. Fig. S5 shows current traces of spHCN/F459L mutant channels with a saturating concentration of 10 μM cAMP. Fig. S6 shows current traces of spHCN/F459L in the presence of 0.5 μM NBD-cAMP. Figs. S7 and S8 show details of a single-exponential fit for results shown in Figs. 2 (E and F) and 3 (C and D). Fig. S9 compares the increase (WT spHCN) or decrease (spHCN/F459L) in fluorescence signal in response to the same set of depolarizing voltage steps. Fig. S10 shows the profile of NBD-cAMP fluorescence intensity in response to the voltage protocol of −80 to +80 and then back to −80 mV. Fig. S11 shows that membrane potential has almost no effects on the fluorescence intensity of NBD-cAMP. Fig. S12 shows dynamic NBD-cAMP binding to the locked-open and locked-closed spHCN channel along a hyperpolarizing voltage step. Figs. S13 and S14 show diminished changes in NBD-cAMP binding to spHCN and mHCN2 channels at high ligand concentrations.

Results

Inactivated spHCN channels show decreased NBD-cAMP binding compared with closed channels

In the absence of cAMP, spHCN channels briefly open in response to hyperpolarizing voltage steps and then quickly inactivate (Fig. 2 A, black trace). Application of cAMP removes this voltage-dependent inactivation and makes the spHCN channel behave like HCN1 or HCN2 channels (Fig. 2 A, red trace; and Fig. 1 B; Gauss et al., 1998; Shin et al., 2004). cAMP increases spHCN current amplitude with an EC50 of 0.74 μM (macroscopic current measured at −100 mV; Gauss et al., 1998). To monitor the dynamic interactions between cAMP and the spHCN channel, we used NBD-cAMP as the fluorescent marker. The fluorescence intensity of NBD increases over 90-fold upon binding to the CNBD (Wu et al., 2011). NBD-cAMP at a concentration of 0.5 μM had a minimal impact on the channel, most likely because of the presence of an extra fluorescence group. With NBD-cAMP in bath solution and membrane potential held at +80 mV, we consistently observed a rundown of fluorescence intensity after the start of the optical recording with laser pulses, which was likely caused by modification of the spHCN channels (Idikuda et al., 2018). To circumvent the issue of PDM, we applied 2 mM Trolox-C to the bath solution when col-

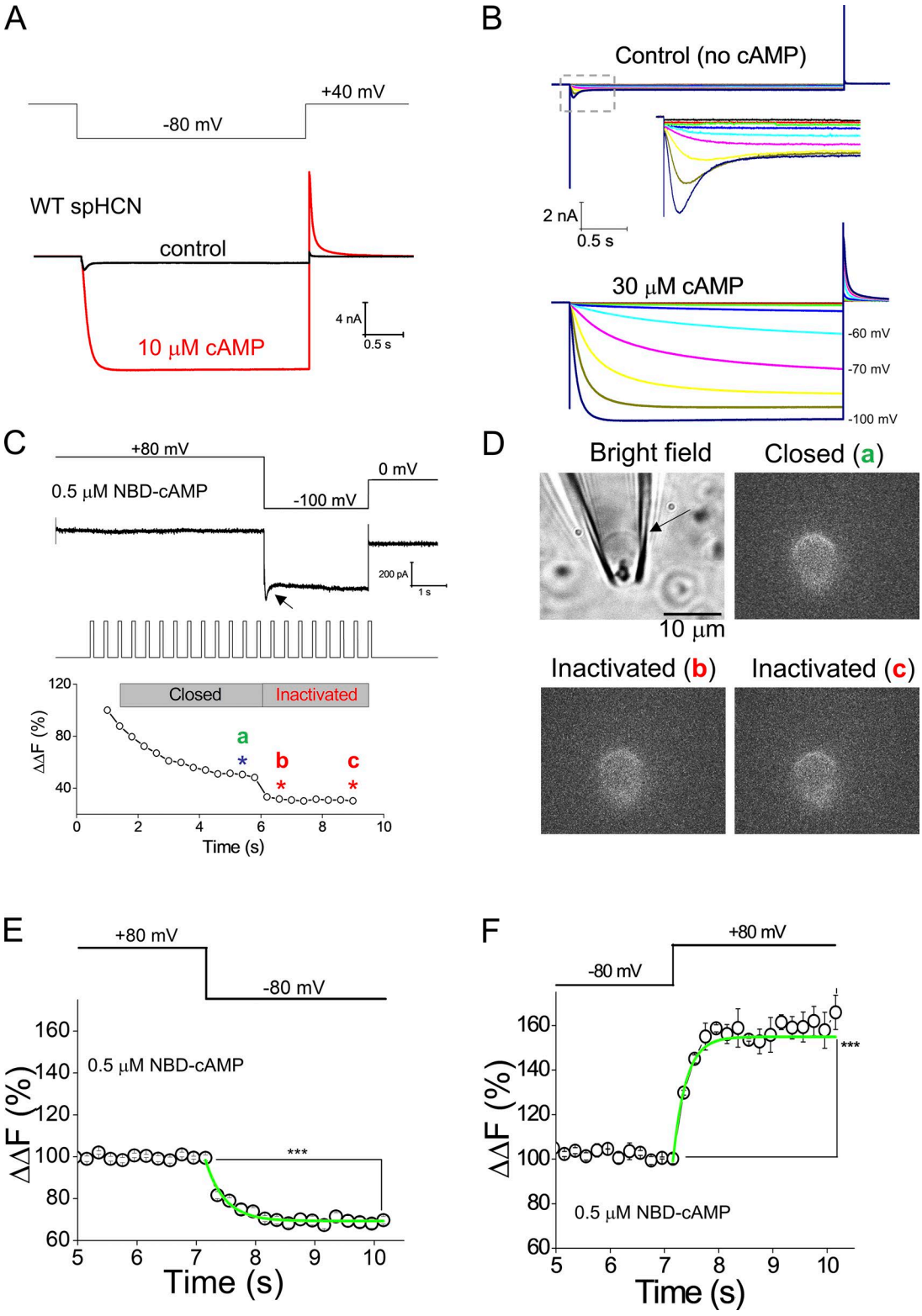

Figure 2. **Inactivated spHCN channels show decreased binding to NBD-cAMP. (A)** In response to a hyperpolarizing voltage step from +40 mV to −80 mV, the WT spHCN channel transiently opens and then inactivates (black trace; no cAMP). Adding cAMP (10 μM) to the bath solution abolishes the inactivation so that the channel shows typical voltage-dependent activation and deactivation (red). **(B)** Current traces of the WT spHCN channel in response to a series of voltage steps from −40 to −130 mV at a −10-mV interval. Top: Current traces in the absence of cAMP. Inset shows a zoomed view over the transient phase of activation–inactivation. Bottom: Current traces with cAMP. **(C)** Raw PCF results of WT spHCN channels. 2 mM Trolox was added to the bath solution to reduce photobleaching and PDM of the channel (Idikuda et al., 2018). The membrane patch was held at 0 mV and then at +80 mV for 6 s to stabilize the optical signal and to let the channel reach a steady state, preceding the hyperpolarizing voltage step from +80 to −100 mV. From top to bottom: Voltage protocol, current trace, laser pulses, and CCD camera exposure protocol, normalized fluorescence intensity. Three representative images (a, b, and c) are shown in D. **(D)** Raw

lecting the results shown in Fig. 2 (C and D). To obtain more stable optical recordings and ensure most channels were in the closed state, we held membrane potential at +80 mV and continued optical recording with laser pulses for 6 s before applying a hyperpolarizing voltage step to −100 mV. Impressively, corresponding to voltage-dependent channel inactivation, a significant reduction in NBD-cAMP binding was observed (with Trolox-C; Fig. 2, C and D).

Experiments were repeated in the absence of Trolox-C but still with a 7-s continuous optical recording at a holding potential of +80 mV. Average results showed that upon the hyperpolarizing step to −80 mV, NBD-cAMP binding to inactivated spHCN channels decreased by 31.4 ± 0.02% compared with the binding to closed channels (Fig. 2 E). The decrease in NBD-cAMP binding was time dependent and could be fit by a single-exponential function. Conversely, upon a depolarizing voltage step from −80 to +80 mV, a significant increase in NBD-cAMP binding was observed (Fig. 2 F). Thus, the dynamic binding of cAMP to spHCN channels upon changes in membrane potential is totally opposite to that of mHCN2 channels, which display a robust increase in both cAMP binding and channel opening in response to a hyperpolarization (Kusch et al., 2010; Wu et al., 2011). We reproduced the same trends by using either a mutant spHCN channel, spHCN/H462A, which showed minimal responses to PDM (Fig. S2), or very short laser pulses (10 ms) and a differently labeled cAMP (FITC-cAMP; Figs. S3 and S4).

spHCN F459L abolishes channel inactivation and reverses the decreased NBD-cAMP binding upon hyperpolarization

F459 is located in the S6 of spHCN and aligned precisely with the first proline of the PVP (proline–valine–proline) motif in voltage-gated potassium channels (Fig. 6 A; Webster et al., 2004). Replacing phenylalanine with leucine (F459L) effectively abolished the voltage-dependent inactivation of spHCN and made the channel behave just like HCN1 or HCN2 (Shin et al., 2004). Upon exposure to cAMP applied to the intracellular side, spHCN/F459L mutant channels showed faster activation and slower deactivation (Fig. 3, A and B; and Fig. S5). Next, using the same PCF protocol as for WT spHCN channels, we studied the binding of NBD-cAMP to spHCN/F459L during channel activation (Fig. 3 C; and Fig. S6, A and B) and deactivation (Fig. 3 D; and Fig. S6, C and D). Indeed, during channel activation, NBD-cAMP binding to spHCN/F459L was increased by 51.1 ± 0.03%, which is similar to that in mHCN2 but opposite to the decrease in NBD-cAMP binding observed in WT spHCN. Conversely, NBD-cAMP binding to spHCN/F459L was decreased by 34.8 ± 0.03% during deactivation, which was similar to that in mHCN2 but again opposite to that in WT spHCN. Thus, the F459L mutation by itself made the spHCN channel behave just like mHCN2 with respects to both voltage-dependent activation/deactivation and dynamic cAMP binding.

For both WT spHCN and spHCN/F459L channels, the time course of the dynamic binding of NBD-cAMP in response to voltage steps were well described by single exponential fits. Examples of curve fitting can be found in Fig. S7 for WT and Fig. S8 for F459L mutant channels, respectively. For WT spHCN, in response to hyperpolarizing voltage steps, the time constant of NBD-cAMP binding decreased approximately threefold, from 0.60 ± 0.04 s at −60 mV to 0.21 ± 0.04 s at −120 mV, suggesting that the binding of NBD-cAMP to the channel is a voltage-driven process (Fig. 4, A–C). As indicated by ΔΔF, the relative decrease in NBD-cAMP binding reached a plateau/steady state near −80 mV, without any further decrease at more negative potentials. For the spHCN/F459L channel, although the direction of the change in NBD-cAMP binding is opposite to that of the WT channel, the time constant for NBD-cAMP binding also is voltage dependent (1.39 ± 0.19 s at −60 mV and 0.83 ± 0.18 s at −120 mV; Fig. 4, D–F). Similarly, the relative increase in NBD-cAMP binding reached a plateau at −80 mV. It is noteworthy that the kinetics of NBD-cAMP binding were much slower than the movement of the voltage sensor, which was largely finished within 50 ms after the start of the hyperpolarizing voltage step (Ryu and Yellen, 2012). The corresponding results of NBD-cAMP binding in response to depolarizing voltage steps for WT and F459L are shown in Fig. S9.

Moreover, we monitored NBD-cAMP binding along a voltage protocol that contained both hyperpolarizing and depolarizing steps (+80 to −80 mV and then back to +80 mV; Fig. S10). The binding of NBD-cAMP recovered to a level that was slightly lower than the starting level, probably because of the bleach of NBD-cAMP. Notably, the binding of NBD-cAMP to the channel was not intrinsically voltage dependent. As shown in Fig. S11, corresponding to the voltage step from −40 to +80 mV (no obvious channel opening), the fluorescence intensity showed no obvious changes in response to a voltage jump of 120 mV.

ZD7288, but not Cs^+, dampens the decrease in NBD-cAMP binding to inactivated spHCN channels

As F459 is located in S6 and close to the activation gate of spHCN, the above results suggested that the movement of the gate should be allosterically coupled to the binding of NBD-cAMP. Previously, to investigate a similar mechanism in mHCN2, we used a specific HCN channel blocker, ZD7288, to introduce local structural perturbations in the vicinity of the activation gate (BoSmith et al., 1993; Wu et al., 2012). The binding site of ZD7288 has been mapped to a region close to the inner activation gate in the spHCN channel and involves residues from S6 (Shin et al., 2001, 2004; Rothberg et al., 2002). To confirm the allosteric communication between the movement of the gate and cAMP binding in WT spHCN, we applied 60 µM ZD7288 to the bath solution and measured the dynamic NBD-cAMP binding in response to

fluorescence images of the membrane patch along the hyperpolarization voltage step (a, b, and c in C). **(E)** Averaged results showing the significant reduction in fluorescence intensity (31.4 ± 0.02%; paired *t* test; P < 0.0001; *n* = 12) upon the voltage step from +80 to −80 mV. The fluorescence intensity was normalized to the averaged value of the last three images before the voltage step. Green trace shows the single-exponential fit of the time-dependent decrease in cAMP binding. **(F)** Averaged results showing a significant recovery in fluorescence intensity (51.1 ± 0.03%; paired *t* test; P < 0.0001; *n* = 12) upon the depolarization voltage step from −80 to +80 mV. Green trace shows the single-exponential fit of the time-dependent increase in fluorescence intensity. Asterisks here and after represent levels of statistical significance (see Statistics in Materials and methods).

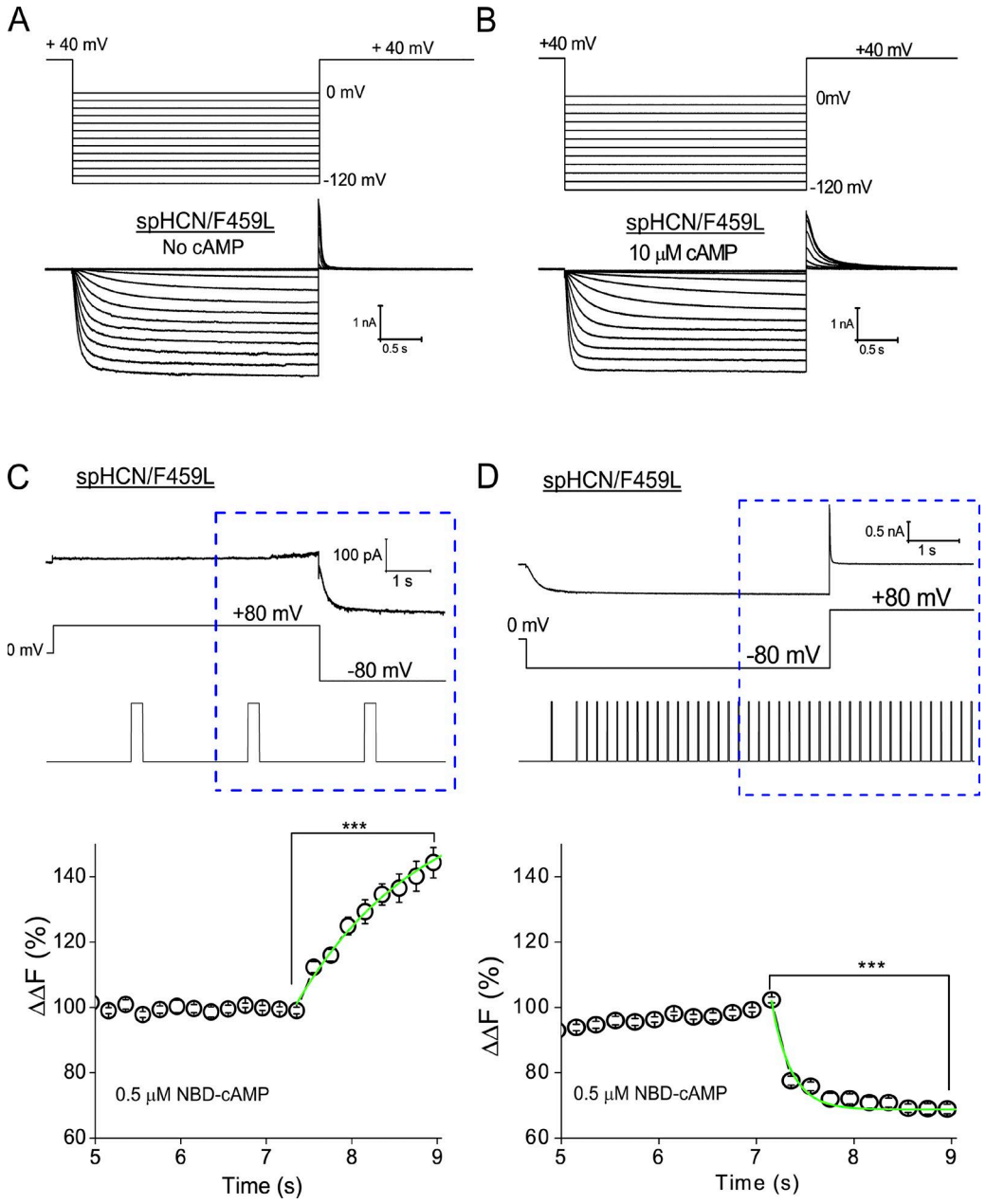

Figure 3. **A single point mutation in S6, F459L, abolishes the channel inactivation and reverses the decrease in NBD-cAMP binding upon membrane hyperpolarization. (A)** Current traces of the spHCN/F459L mutant channel recorded in response to a series of hyperpolarization voltage steps (no cAMP). **(B)** Current traces of the spHCN/F459L channel recorded in the presence of 10 μM cAMP. Notice the changes in channel kinetics (faster activation and slower deactivation) compared with the traces shown in A. **(C)** Top: Current traces of spHCN/F459L in response to the hyperpolarization voltage step from +80 to −80 mV. Bottom: Averaged results corresponding to the dashed blue box shown in C showing a significant increase in ΔΔF upon the voltage step from +80 to −80 mV (58.4 ± 0.05%; paired *t* test; P < 0.0001; *n* = 12). **(D)** Top: Current traces of spHCN/F459L in response to the depolarization voltage step from −80 to +80 mV. Bottom: Averaged results corresponding to the dashed blue box shown in D showing a significant decrease in ΔΔF upon the voltage step from −80 to +80 mV (34.78 ± 0.03%; paired *t* test; P < 0.0001, *n* = 17).

hyperpolarizing voltage steps. Indeed, in the presence of ZD7288, the reduction of NBD-cAMP binding upon hyperpolarization was significantly dampened by ∼10% with ZD7288 versus ∼40% in the absence of ZD7288 at −100 mV (Fig. 5, A–C).

Other than ZD7288, Cs^+ in the millimolar range is another widely used blocker for HCN channels (Fain et al., 1978; Barnes and Hille, 1989). The binding site for Cs^+ has been mapped to the region near the extracellular opening of the ion conducting pore (DiFrancesco, 1982; Denyer and Brown, 1990). We added 2 mM Cs^+ to the pipette solution, which is in contact with the extracellular side of the membrane. In contrast to ZD7288, blocking the ionic current by Cs^+ had no obvious effects on the binding of NBD-cAMP to spHCN channels (Fig. 5, D–F).

Locked-open and locked-closed spHCN channels show opposite changes in NBD-cAMP binding

It has been proposed that inactivation of spHCN is caused by reclosure of the activation gate near S6 (Shin et al., 2004). The

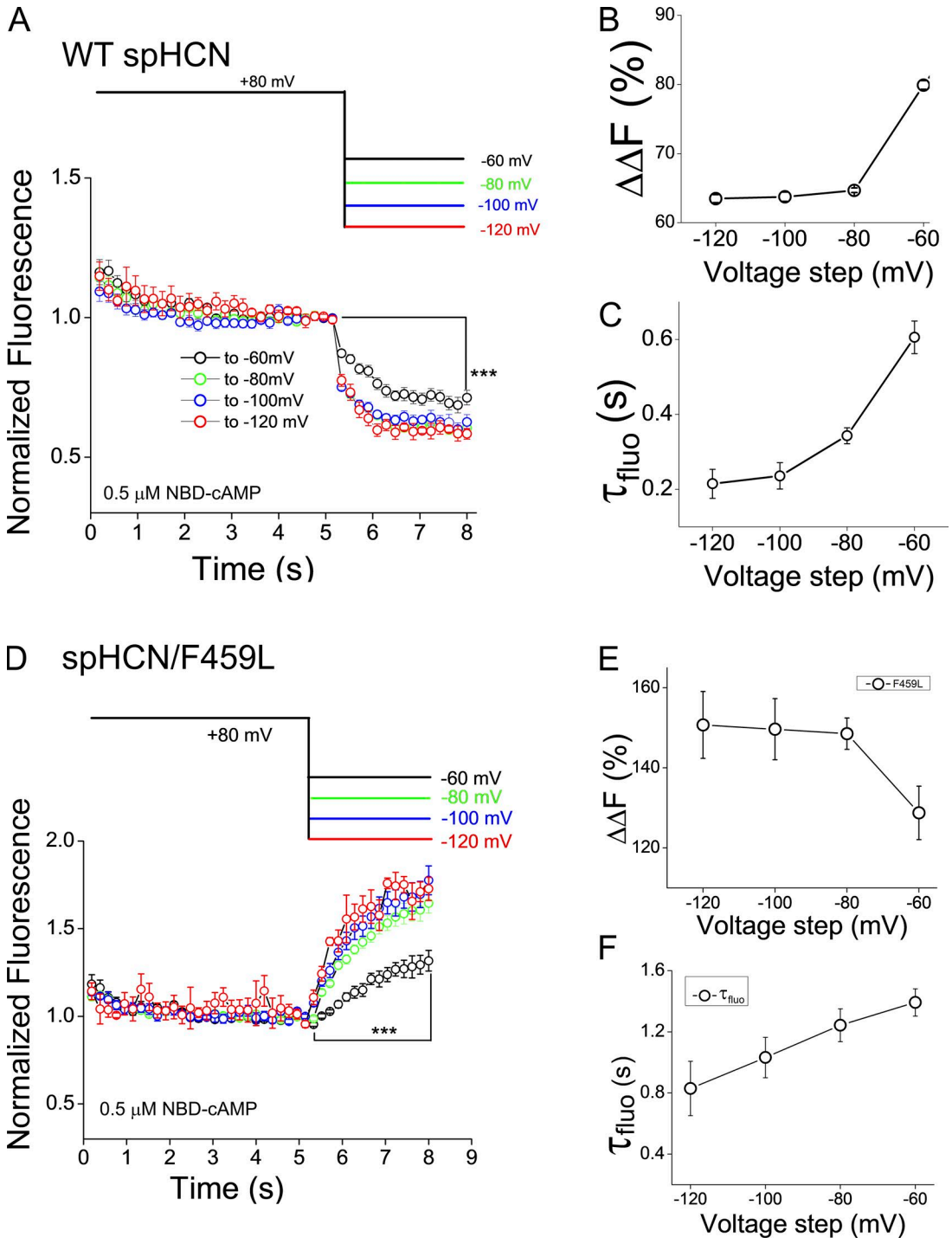

Figure 4. **Comparing the decrease (WT spHCN) or increase (spHCN/F459L) in NBD-cAMP binding in response to the same set of hyperpolarization voltage steps. (A)** The membrane patches were held at +80 mV for 5 s before the application of hyperpolarization voltage steps from −60 to −120 mV at a −20-mV interval. Fluorescence intensities for each patch were normalized to the value of the last three images just before the voltage steps. At −60 mV, paired *t* test: P < 0.0001, *n* = 12. **(B)** Percentage of the decreases in fluorescence intensity versus hyperpolarization voltage steps. Averaged results of the WT spHCN channel shown in A are used in the calculation. **(C)** Time constant of the decrease in fluorescence intensity of the WT spHCN channel versus hyperpolarization voltage steps. The profiles of the decrease in fluorescence intensity after the hyperpolarization voltage steps shown in A were fitted by a single-exponential function. **(D)** Normalized fluorescence intensity for the spHCN/F459L mutant channel. At −60 mV, paired *t* test: P < 0.0001, *n* = 13. **(E)** Percentage of the increases in fluorescence intensity of the spHCN/H462A mutant channel versus hyperpolarization voltage steps. Averaged results shown in D are used in the calculation. **(F)** Time constant of the increase in fluorescence intensity of the spHCN/H462A channel versus hyperpolarization voltage steps. Profiles of the increase in fluorescence intensity after hyperpolarization voltage steps shown in D were fitted by a single-exponential function.

decrease in NBD-cAMP binding to inactivated spHCN could be a direct consequence of this rapid reclosure of the gate. Therefore, it will be interesting to directly compare the binding of NBD-cAMP to spHCN channels in three different functional

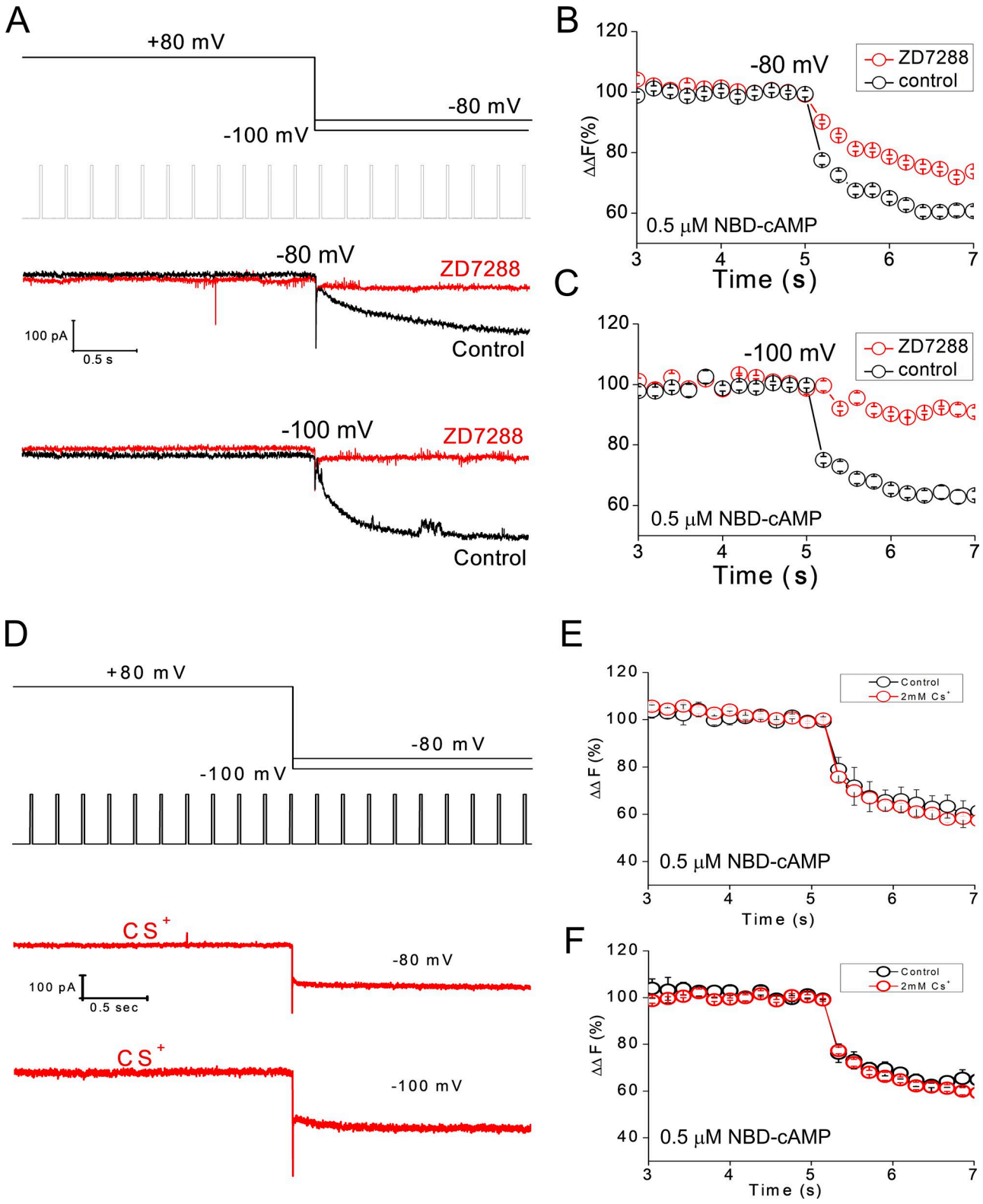

Figure 5. **Both ZD7288 and Cs^+ can block the spHCN current, but only ZD7288 affects the binding of NBD-cAMP. (A)** ZD7288 blocks the currents of the WT spHCN channel. Top: Voltage step, laser pulse, and image collection protocol. Bottom: Current traces before (black) and after (red) adding 60 μM ZD7288. **(B)** Normalized fluorescence intensity before (black) and after (red) ZD7288 application. Voltage step, +80 to −80 mV (n = 17). **(C)** Normalized fluorescence intensity before (black) and after (red) ZD7288 application. Voltage step, +80 to −100 mV. **(D)** 2 mM Cs^+ was added to the pipette solution to block the WT spHCN current from the extracellular side. Top: Voltage step, laser pulse, and image collection protocol. Bottom: Current traces collected with Cs^+ added to the pipette solution. **(E)** Normalized fluorescence intensity without (black) or with Cs^+ (red). Voltage step, +80 to −80 mV. Because the pipette solution was not exchanged during the experiments, control results and Cs^+ results were collected from different patches (n = 13). **(F)** Normalized fluorescence intensity without (black) or with Cs^+ (red). Voltage step, +80 to −80 mV.

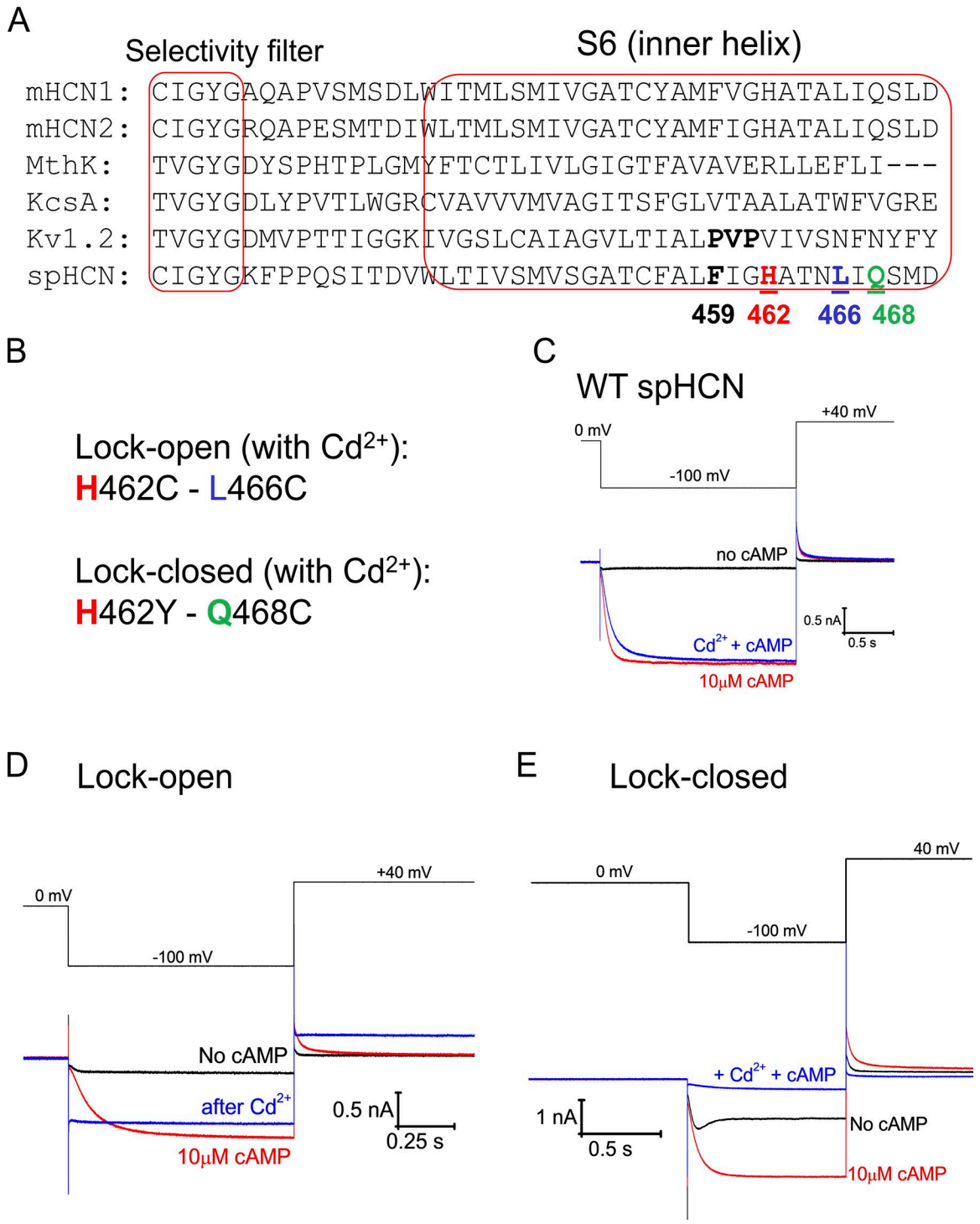

Figure 6. **Strategy to specifically lock the spHCN channel in either the open or closed state. (A)** Alignment of primary protein sequences of representative HCN and other potassium channels in the region encompassing the selectivity filter and the last transmembrane segment (S2 in KcsA or S6 in other channels). Relevant residues are shown in bold and marked with a different color. **(B)** Mutations introduced to the S6 of the spHCN channel to make the locked-open (H462C-L466C) or locked-closed (H462Y-Q468C) channel. **(C)** Current traces of the WT spHCN channel. Black, control in the absence of cAMP and Cd^{2+}. Red, 10 μM cAMP. Blue, 10 μM cAMP and 1μM Cd^{2+}. **(D)** Current traces of the locked-open spHCN channel. Black, control in the absence of cAMP and Cd^{2+}. Red, 10 μM cAMP. Blue, 1 μM Cd^{2+} without cAMP. The locked-open effect was persistent after the washing off of cAMP (bath solution containing Cd^{2+}). **(E)** Current traces of the locked-closed spHCN channel. Black, control in the absence of cAMP and Cd^{2+}. Red, 10 μM cAMP. Blue, 2 μM Cd^{+2} and 10 μM cAMP.

states: closed, inactivated, and open. To this end, we adopted the strategy of specifically "locking" spHCN in open or closed states by applying Cd^{2+} to cysteine-replacement mutant channels (spHCN/H462C-L466C to locked-open or spHCN/H462Y-Q468C to locked-closed; Rothberg et al., 2002, 2003; Fig. 6, A and B). For WT spHCN, cAMP is required to maintain the open state, re-

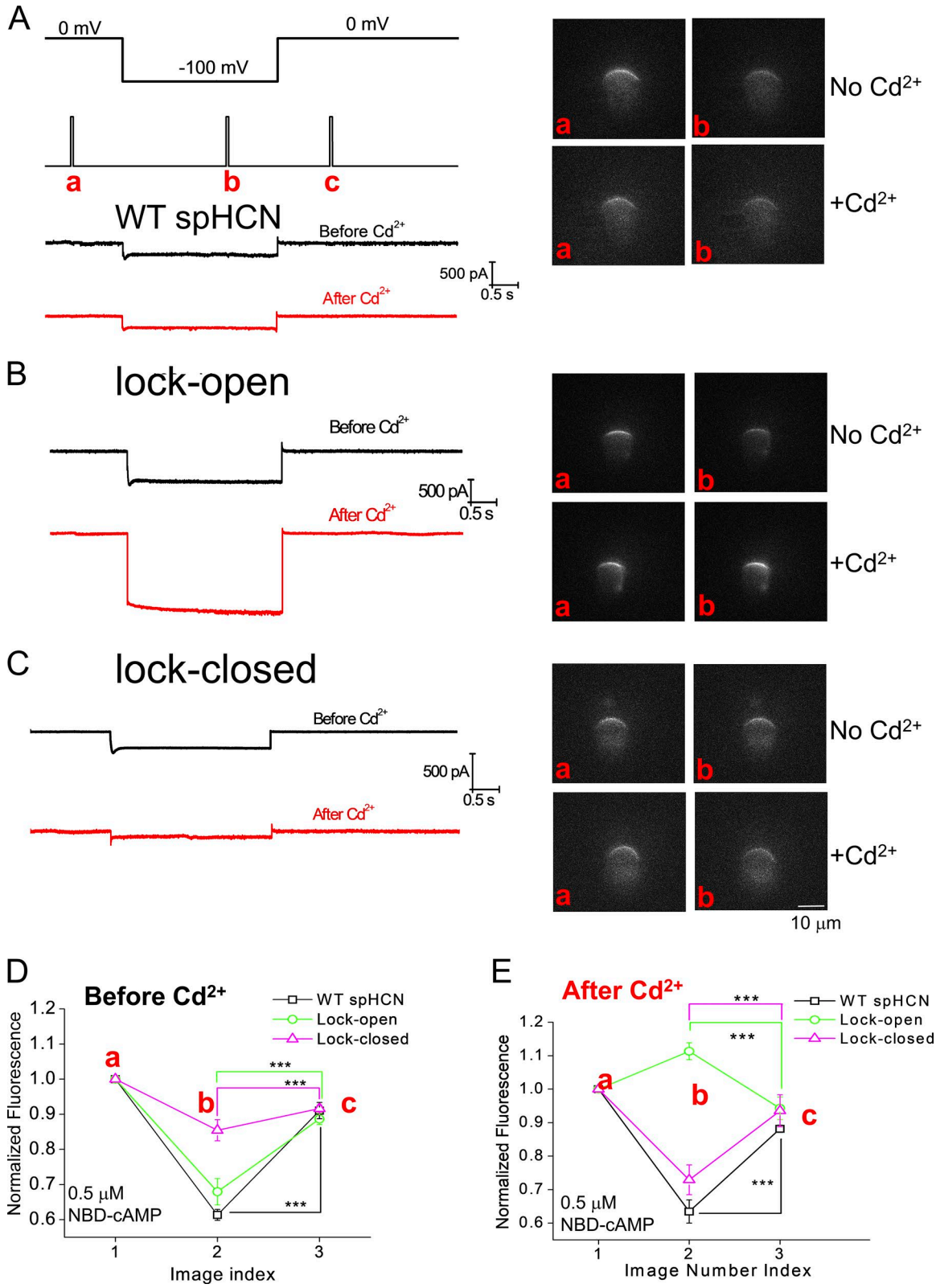

Figure 7. **The inactivated WT spHCN channel, the locked-open spHCN channel and the locked-closed spHCN channel show three different levels of binding to NBD-cAMP. (A)** Current traces and original fluorescence images of the WT spHCN channel. Left top: Voltage step, laser pulse, and image collection protocol. The time of three images (a, b, and c) is indicated. Left bottom: Current traces before and after Cd^{2+}. Right: Images collected before (top) and after (bottom) Cd^{2+} application. **(B)** Results of the locked-open spHCN channel. The same experimental protocol as used for the WT spHCN channel was applied. **(C)** Results of the locked-closed spHCN channel. The same experimental protocol as used for the WT spHCN channel was applied. **(D)** Normalized fluorescence intensity of the WT (black), locked-open (green), and locked-closed (magenta) spHCN channels before Cd^{2+} application. Results were normalized to the fluorescence intensity of image a. Before the application of Cd^{2+}, all channels show a decrease in cAMP binding upon the hyperpolarization voltage step from 0

gardless of the absence or presence of Cd^{2+} (1 μM on top of cAMP; Fig. 6 C). For locked-open or locked-closed channels, exposure to Cd^{2+} (1 or 2 μM, correspondingly; in the absence of cAMP) traps the channel in either the open or closed state (Fig. 6, D and E). Red traces show the maximal opening of the channel in the presence of 10 μM cAMP before application of Cd^{2+}.

Next, we investigated the binding of NBD-cAMP to locked-open or locked-closed spHCN channels. Because of the instability of the membrane seal in the presence of Cd^{2+} and the issue of dye photobleaching, we used a simple protocol of collecting only three images (before, during, and after the step to −100 mV) and repeated the same protocol before and after applying Cd^{2+} (Fig. 7 A). Notably, we ran into issues of patch stability because of longer recording time and the application of Cd^{2+}. A holding potential of 0 mV was chosen to reduce the damage to membrane seal upon stepping to −100 mV. This should not significantly affect the interpretation, because both the voltage sensor movement and opening of spHCN channels were minimal between holding potentials of −20 and +80 mV (Bruening-Wright et al., 2007).

Before the application of Cd^{2+}, for all three cases (WT, locked-open, and locked-closed spHCN), NBD-cAMP binding decreased during the step to −100 mV and recovered upon stepping back to 0 mV. Impressively, 1 μM Cd^{2+} switched the direction of dynamic NBD-cAMP binding to locked-open channels from a decrease to increase during the step to −100 mV (Fig. 7 B). In contrast, after the application of 2 μM Cd^{2+} to lock the channels in the closed state (locked-closed), NBD-cAMP binding still decreased in response to hyperpolarization but was maintained at a level greater than that for inactivated WT spHCN channel (Fig. 7, C–E). The corresponding measurements of the kinetics of NBD-cAMP binding to WT, locked-open, and locked-closed channels are shown in Fig. S12. Collectively, these results clearly demonstrate differences in the dynamic binding of NBD-cAMP to spHCN channels in the closed, inactivated, and open states.

Discussion

By bridging membrane excitability with intracellular signaling pathways, HCN channels play important roles in the nervous and cardiovascular systems. At the molecular level, dually voltage- and ligand-regulated HCN channels are an elegant model for studying ion channel protein allostery. Here, we addressed the allosteric coupling of the activation/inactivation gate upon cAMP binding in full-length spHCN channels, using fluorescent cAMP as the marker for cAMP binding. Surprisingly, cAMP binding to spHCN channel decreases in response to hyperpolarizing voltage steps. We further investigated the allosteric communication between the gate and cAMP binding in spHCN channels from three directions: (1) using the spHCN/F459L mutant channel that does not show inactivation; (2) applying ZD7288, a blocker of which the binding site has been mapped to the area near the activation gate; and (3) adopting the strategy of locking the channel in either open or closed state. The experimental results provided direct support for allosteric communication between the activation gate and cAMP binding and demonstrated distinct levels of cAMP binding to the closed, inactivated, and open states of the channel.

Our approach to assess the state-dependent binding of NBD-cAMP to a pool of channels expressed on a membrane patch is comparable to equilibrium-based biochemical binding assays. To this end, it is important but always challenging to specifically lock the protein in a certain state and then determine the binding affinity for this particular state. The voltage dependence of the spHCN channel and the strategy to specifically lock channels in either the open or closed state make it possible to specifically measure the binding of NBD-cAMP to a group of channels predominately in a defined state. However, several potential issues regarding the application of fluorescently labeled cAMP also need to be considered. In this study, we mainly used NBD-cAMP as the fluorescent marker. NBD is unique in that its fluorescence dramatically increases upon the transition from an aqueous environment to the hydrophobic binding pocket in CNBD (Wu et al., 2011). To exclude the possibility that changes in the local chemical environment affected NBD fluorescence, we assessed the spHCN binding of FITC-cAMP, a fluorophore with a totally different chemical structure from NBD. The results of FITC-cAMP corroborated the results with NBD-cAMPs. Moreover, both fluorophores are attached to the 8′ carbon in the adenine group, whereas the negatively charged cyclic phosphate is attached to the sugar base at a distance from the adenine group. The cyclic phosphate moiety plays a critical role in binding by interacting with a highly conserved arginine residue in CNBD (R620 in spHCN and R591 in mHCN2). Another important issue is the efficacy of fluorescently labeled cAMP binding on channel function. Previously, we used NBD-cAMP to study mHCN2 channels and confirmed that NBD-cAMP and cAMP exert similar regulatory effects on this channel isoform (Wu et al., 2011). However, NBD-cAMP was less effective in regulating the function of spHCN channels. Optimally, the fluorescently labeled cAMP molecules that exert regulatory effects comparable to cAMP and exhibit fluorescence characteristics suitable for PCF might reduce any ambiguity in the interpretation of experimental results.

It is recognized that at subsaturating levels of NBD-cAMP (0.5–1 μM for spHCN), only a fraction of the channels on the membrane patch are complexed with NBD-cAMP. Thus, a mismatch might exist between the fluorescence signal generated by the fraction of channels complexed with NBD-cAMP and the electrical signal generated by all channels on the membrane, wherein NBD-cAMP–bound and unbound channels might behave differently. We compared the changes in fluorescence between two concentrations of NBD-cAMP: 1 μM and 10 μM. In contrast to the decrease in fluorescence intensity with 1 μM

to −100 mV and a significant recovery after the depolarization voltage step from −100 to 0 mV ($P < 0.001$). **(E)** Normalized fluorescence intensity of the WT (black, $n = 6$), locked-open (green, $n = 8$), and locked-closed (magenta, $n = 8$) spHCN channels after Cd^{2+} application. After the application of Cd^{2+}, the WT and the locked-closed channels still show similar trend of decrease in fluorescence intensity, whereas the locked-open channel shows a significant increase ($P < 0.001$) in fluorescence intensity.

NBD-cAMP, no obvious changes in fluorescence intensity were detected with 10 μM NBD-cAMP (Fig. S13). The optical detection system was operating in the linear range, as the maximal intensity of the fluorescence signal was <20% of the saturating level. This result is reminiscent of the observations with mouse HCN2 channels. Under subsaturating concentrations of NBD-cAMP (0.05 or 0.1 μM), there was a significant increase in fluorescence intensity (binding) corresponding to membrane hyperpolarization. However, further increasing the concentration of NBD-cAMP to 3 μM dramatically reduced the increase in NBD-cAMP binding (Fig. S14). This observation was previously reported in published studies on HCN2 channels (Kusch et al., 2010, 2011; Wu et al., 2011). Therefore, higher concentrations of ligand diminish the difference in ligand binding among different functional states. It is notable that for spHCN channels NBD-cAMP has a reduced efficacy and potentially binding affinity compared with regular cAMP.

Clearly, the decrease in NBD-cAMP binding to WT spHCN channel upon membrane hyperpolarization is a voltage-dependent process, as indicated by the decrease in the time constant from ∼0.6 s at −60 mV to ∼0.2 s at −120 mV (Fig. 4 C). A direct coupling mechanism should exist between the movement of the voltage sensor and cAMP binding. However, the S4 may or may not directly communicate with the CNBD, because the kinetics of dynamic cAMP binding are much slower than the movement of the voltage sensor. Previous gating current measurements in spHCN demonstrated that the majority of charge displacement finishes within 50 ms after the voltage step, whereas more time (hundreds of milliseconds) is required for NBD-cAMP binding to reach a plateau (Bruening-Wright et al., 2007; Ryu and Yellen, 2012). Therefore, it is likely that structural rearrangements downstream from the movement of S4 affect the binding of cAMP. As supported by our results, it is very likely the movement of the gate in S6 plays a critical role in the allosteric modulation of cAMP binding and simultaneously controls the opening or closing of the ion-conducting pathway.

In the absence of cAMP, the spHCN/F459L channel behaves just like the mHCN1 or mHCN2 channels. Sequence alignment shows that F459 is aligned to the first proline in the critical PVP motif in the S6 of Kv channels and is very close to the proposed activation gate for HCN channels (del Camino et al., 2000; Zhou et al., 2001; Hackos et al., 2002; Rothberg et al., 2002, 2003; Webster et al., 2004). Our observations with the spHCN/F459L mutant channel are quite intriguing, because a single mutation effectively abolishes the voltage-dependent inactivation and concurrently switches the direction of NBD-cAMP binding from a decrease in inactivated WT spHCN channels to an increase in "normally opening" F459L mutant channels. Alanine replacement of the corresponding residue in the mHCN2 channel, F431A, reduced NBD-cAMP binding and prolonged channel deactivation, which might share certain mechanistic connections with spHCN/F459L (Wu et al., 2012). The location of F459, close to the activation gate and in close contact with a critical hydrophobic pocket formed by residues from the S4–S5 linker of a neighboring subunit, is reminiscent of the disease-causing L269F mutation in the muscle-type nicotinic AChR epsilon subunit (Engel et al., 1996; Colomer et al., 2006; Piccari et al., 2011). The L269F mutation causes pathological channel openings in the absence of ACh and excessive Ca^{2+} entry. L269 has been shown to be critical for the ligand-dependent gating in AChR (Purohit and Auerbach, 2011; Jha et al., 2012). Interestingly, L269 is located in the m2 segment in AChR that aligns with the ionic conducting pore, just like the S6 helix in Kv or HCN channels, and also engages in hydrophobic interactions with neighboring subunits.

To further delineate the binding of cAMP under different functional states, we adopted the strategy of locking the spHCN channel in either the open or closed state (Rothberg et al., 2003; Shin et al., 2004). Gating currents recorded from these gate-locked channels still showed a certain dependency on voltage, indicating a weak coupling between the gate and the movement of the voltage sensor (Ryu and Yellen, 2012). It was shown that the Q-V curves of the locked-open and locked-closed spHCN channel shift in opposite directions, which confirmed the impacts of the immobilized gate on S4 and thus the retrograde communication between the gate and the voltage sensor. Such retrograde communication has been reported for NaV channels (Muroi et al., 2010). Here, from the perspective of ligand-dependent gating, our measurements of NBD-cAMP binding to locked-open or locked-closed spHCN channels, together with a previous study of state-dependent binding of NBD-cAMP to mHCN2 channels, complement investigations on the allosteric communication between the gate and the voltage sensor in voltage-gated channels.

In summary, we used fluorescent cAMP as the marker for cAMP binding and confirmed that the interaction between cAMP and the spHCN channel is dynamic and depends on functional state (closed, inactivated, and open). We obtained direct evidence for the allosteric communication between the activation/inactivation gate located near the intracellular end of S6 and CNBD. As an important negative feedback mechanism, voltage-dependent inactivation and ligand-dependent desensitization are gating mechanisms frequently adopted by diverse types of channels and receptors. By targeting the ligand binding in inactivated spHCN channels, our study provides useful insights for the mechanistic interpretation of inactivation and desensitization. Importantly, the intimate coordination among adjacent and discrete domains and interpretation at the whole-molecule level still should be an important direction to pursue for understanding allosteric effects in proteins.

Acknowledgments

We acknowledge technical support from C. Xie and T. Zhao and are grateful for the complementary DNA sample encoding the spHCN channel from Drs. Reinhard Seifert and U. Benjamin Kaupp (Center of Advanced European Studies and Research). We thank Dr. C. Baumgarten and Dr. R. Pittman for their insightful comments on the manuscript and their help with writing.

This work was supported by the National Institute of Health (grants R01GM098592 and R01GM109193) and Virginia Commonwealth University (startup funds to Q. Liu and L. Zhou).

The authors declare no competing financial interests.

Author contributions: V. Idikuda, W. Gao, and Z. Su performed the experiments and analyzed the data. Q. Liu and L. Zhou analyzed the data and supervised the project. Chemical structures

were downloaded from Wikipedia. All authors participated in writing the manuscript.

Kenton J. Swartz served as editor.

Submitted: 2 February 2018
Revised: 8 July 2018
Accepted: 13 November 2018

References

Barnes, S., and B. Hille. 1989. Ionic channels of the inner segment of tiger salamander cone photoreceptors. *J. Gen. Physiol.* 94:719–743. https://doi.org/10.1085/jgp.94.4.719

Biel, M., C. Wahl-Schott, S. Michalakis, and X. Zong. 2009. Hyperpolarization-activated cation channels: from genes to function. *Physiol. Rev.* 89:847–885. https://doi.org/10.1152/physrev.00029.2008

Biskup, C., J. Kusch, E. Schulz, V. Nache, F. Schwede, F. Lehmann, V. Hagen, and K. Benndorf. 2007. Relating ligand binding to activation gating in CNGA2 channels. *Nature.* 446:440–443. https://doi.org/10.1038/nature05596

BoSmith, R.E., I. Briggs, and N.C. Sturgess. 1993. Inhibitory actions of ZENECA ZD7288 on whole-cell hyperpolarization activated inward current (If) in guinea-pig dissociated sinoatrial node cells. *Br. J. Pharmacol.* 110:343–349. https://doi.org/10.1111/j.1476-5381.1993.tb13815.x

Bruening-Wright, A., F. Elinder, and H.P. Larsson. 2007. Kinetic relationship between the voltage sensor and the activation gate in spHCN channels. *J. Gen. Physiol.* 130:71–81. https://doi.org/10.1085/jgp.200709769

Colomer, J., J.S. Müller, A. Vernet, A. Nascimento, M. Pons, V. Gonzalez, A. Abicht, and H. Lochmüller. 2006. Long-term improvement of slow-channel congenital myasthenic syndrome with fluoxetine. *Neuromuscul. Disord.* 16:329–333. https://doi.org/10.1016/j.nmd.2006.02.009

Craven, K.B., and W.N. Zagotta. 2006. CNG and HCN channels: two peas, one pod. *Annu. Rev. Physiol.* 68:375–401. https://doi.org/10.1146/annurev.physiol.68.040104.134728

del Camino, D., M. Holmgren, Y. Liu, and G. Yellen. 2000. Blocker protection in the pore of a voltage-gated K+ channel and its structural implications. *Nature.* 403:321–325. https://doi.org/10.1038/35002099

Denyer, J.C., and H.F. Brown. 1990. Pacemaking in rabbit isolated sino-atrial node cells during Cs+ block of the hyperpolarization-activated current if. *J. Physiol.* 429:401–409. https://doi.org/10.1113/jphysiol.1990.sp018264

DiFrancesco, D. 1982. Block and activation of the pace-maker channel in calf purkinje fibres: effects of potassium, caesium and rubidium. *J. Physiol.* 329:485–507. https://doi.org/10.1113/jphysiol.1982.sp014315

DiFrancesco, D. 1985. The cardiac hyperpolarizing-activated current, if. Origins and developments. *Prog. Biophys. Mol. Biol.* 46:163–183. https://doi.org/10.1016/0079-6107(85)90008-2

Engel, A.G., K. Ohno, M. Milone, H.L. Wang, S. Nakano, C. Bouzat, J.N. Pruitt II, D.O. Hutchinson, J.M. Brengman, N. Bren, et al. 1996. New mutations in acetylcholine receptor subunit genes reveal heterogeneity in the slow-channel congenital myasthenic syndrome. *Hum. Mol. Genet.* 5:1217–1227. https://doi.org/10.1093/hmg/5.9.1217

Fain, G.L., F.N. Quandt, B.L. Bastian, and H.M. Gerschenfeld. 1978. Contribution of a caesium-sensitive conductance increase to the rod photoresponse. *Nature.* 272:467–469. https://doi.org/10.1038/272467a0

Gauss, R., R. Seifert, and U.B. Kaupp. 1998. Molecular identification of a hyperpolarization-activated channel in sea urchin sperm. *Nature.* 393:583–587. https://doi.org/10.1038/31248

Hackos, D.H., T.H. Chang, and K.J. Swartz. 2002. Scanning the intracellular S6 activation gate in the shaker K+ channel. *J. Gen. Physiol.* 119:521–531. https://doi.org/10.1085/jgp.20028569

Idikuda, V., W. Gao, K. Grant, Z. Su, Q. Liu, and L. Zhou. 2018. Singlet oxygen modification abolishes voltage-dependent inactivation of the sea urchin spHCN channel. *J. Gen. Physiol.* 150:1273–1286. https://doi.org/10.1085/jgp.201711961

Jha, A., S. Gupta, S.N. Zucker, and A. Auerbach. 2012. The energetic consequences of loop 9 gating motions in acetylcholine receptor-channels. *J. Physiol.* 590:119–129. https://doi.org/10.1113/jphysiol.2011.213892

Kusch, J., C. Biskup, S. Thon, E. Schulz, V. Nache, T. Zimmer, F. Schwede, and K. Benndorf. 2010. Interdependence of receptor activation and ligand binding in HCN2 pacemaker channels. *Neuron.* 67:75–85. https://doi.org/10.1016/j.neuron.2010.05.022

Kusch, J., S. Thon, E. Schulz, C. Biskup, V. Nache, T. Zimmer, R. Seifert, F. Schwede, and K. Benndorf. 2011. How subunits cooperate in cAMP-induced activation of homotetrameric HCN2 channels. *Nat. Chem. Biol.* 8:162–169. https://doi.org/10.1038/nchembio.747

Lee, C.H., and R. MacKinnon. 2017. Structures of the Human HCN1 Hyperpolarization-Activated Channel. *Cell.* 168:111–120.e11. https://doi.org/10.1016/j.cell.2016.12.023

Lolicato, M., M. Nardini, S. Gazzarrini, S. Möller, D. Bertinetti, F.W. Herberg, M. Bolognesi, H. Martin, M. Fasolini, J.A. Bertrand, et al. 2011. Tetramerization dynamics of C-terminal domain underlies isoform-specific cAMP gating in hyperpolarization-activated cyclic nucleotide-gated channels. *J. Biol. Chem.* 286:44811–44820. https://doi.org/10.1074/jbc.M111.297606

Ludwig, A., X. Zong, M. Jeglitsch, F. Hofmann, and M. Biel. 1998. A family of hyperpolarization-activated mammalian cation channels. *Nature.* 393:587–591. https://doi.org/10.1038/31255

Lüthi, A., and D.A. McCormick. 1998. H-current: properties of a neuronal and network pacemaker. *Neuron.* 21:9–12. https://doi.org/10.1016/S0896-6273(00)80509-7

Männikkö, R., F. Elinder, and H.P. Larsson. 2002. Voltage-sensing mechanism is conserved among ion channels gated by opposite voltages. *Nature.* 419:837–841. https://doi.org/10.1038/nature01038

Männikkö, R., S. Pandey, H.P. Larsson, and F. Elinder. 2005. Hysteresis in the voltage dependence of HCN channels: conversion between two modes affects pacemaker properties. *J. Gen. Physiol.* 125:305–326. https://doi.org/10.1085/jgp.200409130

Muroi, Y., M. Arcisio-Miranda, S. Chowdhury, and B. Chanda. 2010. Molecular determinants of coupling between the domain III voltage sensor and pore of a sodium channel. *Nat. Struct. Mol. Biol.* 17:230–237. https://doi.org/10.1038/nsmb.1749

Nache, V., T. Eick, E. Schulz, R. Schmauder, and K. Benndorf. 2013. Hysteresis of ligand binding in CNGA2 ion channels. *Nat. Commun.* 4:2866. https://doi.org/10.1038/ncomms3866

Piccari, V., C. Deflorio, R. Bigi, F. Grassi, and S. Fucile. 2011. Modulation of the Ca(2+) permeability of human endplate acetylcholine receptor-channel. *Cell Calcium.* 49:272–278. https://doi.org/10.1016/j.ceca.2011.03.002

Purohit, P., and A. Auerbach. 2011. Glycine hinges with opposing actions at the acetylcholine receptor-channel transmitter binding site. *Mol. Pharmacol.* 79:351–359. https://doi.org/10.1124/mol.110.068767

Robinson, R.B., and S.A. Siegelbaum. 2003. Hyperpolarization-activated cation currents: from molecules to physiological function. *Annu. Rev. Physiol.* 65:453–480. https://doi.org/10.1146/annurev.physiol.65.092101.142734

Rothberg, B.S., K.S. Shin, P.S. Phale, and G. Yellen. 2002. Voltage-controlled gating at the intracellular entrance to a hyperpolarization-activated cation channel. *J. Gen. Physiol.* 119:83–91. https://doi.org/10.1085/jgp.119.1.83

Rothberg, B.S., K.S. Shin, and G. Yellen. 2003. Movements near the gate of a hyperpolarization-activated cation channel. *J. Gen. Physiol.* 122:501–510. https://doi.org/10.1085/jgp.200308928

Ryu, S., and G. Yellen. 2012. Charge movement in gating-locked HCN channels reveals weak coupling of voltage sensors and gate. *J. Gen. Physiol.* 140:469–479. https://doi.org/10.1085/jgp.201210850

Santoro, B., D.T. Liu, H. Yao, D. Bartsch, E.R. Kandel, S.A. Siegelbaum, and G.R. Tibbs. 1998. Identification of a gene encoding a hyperpolarization-activated pacemaker channel of brain. *Cell.* 93:717–729. https://doi.org/10.1016/S0092-8674(00)81434-8

Schneider, C.A., W.S. Rasband, and K.W. Eliceiri. 2012. NIH Image to ImageJ: 25 years of image analysis. *Nat. Methods.* 9:671–675. https://doi.org/10.1038/nmeth.2089

Shin, K.S., B.S. Rothberg, and G. Yellen. 2001. Blocker state dependence and trapping in hyperpolarization-activated cation channels: evidence for an intracellular activation gate. *J. Gen. Physiol.* 117:91–102. https://doi.org/10.1085/jgp.117.2.91

Shin, K.S., C. Maertens, C. Proenza, B.S. Rothberg, and G. Yellen. 2004. Inactivation in HCN channels results from reclosure of the activation gate: desensitization to voltage. *Neuron.* 41:737–744. https://doi.org/10.1016/S0896-6273(04)00083-2

Webster, S.M., D. Del Camino, J.P. Dekker, and G. Yellen. 2004. Intracellular gate opening in Shaker K+ channels defined by high-affinity metal bridges. *Nature.* 428:864–868. https://doi.org/10.1038/nature02468

Wu, S., Z.V. Vysotskaya, X. Xu, C. Xie, Q. Liu, and L. Zhou. 2011. State-dependent cAMP binding to functioning HCN channels studied by patch-clamp fluorometry. *Biophys. J.* 100:1226–1232. https://doi.org/10.1016/j.bpj.2011.01.034

Wu, S., W. Gao, C. Xie, X. Xu, C. Vorvis, F. Marni, A.R. Hackett, Q. Liu, and L. Zhou. 2012. Inner activation gate in S6 contributes to the state-dependent binding of cAMP in full-length HCN2 channel. *J. Gen. Physiol.* 140:29–39. https://doi.org/10.1085/jgp.201110749

Xu, X., Z.V. Vysotskaya, Q. Liu, and L. Zhou. 2010. Structural basis for the cAMP-dependent gating in the human HCN4 channel. *J. Biol. Chem.* 285:37082–37091. https://doi.org/10.1074/jbc.M110.152033

Zagotta, W.N., N.B. Olivier, K.D. Black, E.C. Young, R. Olson, and E. Gouaux. 2003. Structural basis for modulation and agonist specificity of HCN pacemaker channels. *Nature.* 425:200–205. https://doi.org/10.1038/nature01922

Zheng, J., and W.N. Zagotta. 2003. Patch-clamp fluorometry recording of conformational rearrangements of ion channels. *Sci. STKE.* 2003:PL7.

Zhou, M., J.H. Morais-Cabral, S. Mann, and R. MacKinnon. 2001. Potassium channel receptor site for the inactivation gate and quaternary amine inhibitors. *Nature.* 411:657–661. https://doi.org/10.1038/35079500